Supporting Information

Kimura and Kimura 10.1073/pnas.1013275108

SI Materials and Methods

***C. elegans* Strains.** The following strains were used in this study: RT130 *pwIs23[vit-2::gfp]*, AZ244 *unc-119(ed3) III; ruIs57[unc-119(+); pie-1p::gfp::tubulin],* TH27 *unc-119(ed3) III; ddIs6-[unc-119(+); pie-1p::gfp::tbg-1],* JA1403 *unc-119(e2498); weIs15 [unc-119(+); pie-1p::gfp::FYVE*2],* OD179 *unc-119(ed3) III; ltIs79 [pAA196; pie-1p::mCherry::rab-5; unc-119 (+)],* SA141 *unc-119(ed3) III; tjIs8 [pie-1p::gfp::ebp-1; unc-119 (+)],* ONA1 *zyg12(ct350) II; unc-119(ed3) III; ruIs57[unc-119(+); pie-1p::gfp::tubulin],* CAL0092 *unc-119(ed3) III; ddIs6; weIs15,* and CAL0135 *unc-119(ed3) III; wjIs15 [unc-119(+); pie-1p::gfp::dyrb-1]*. CAL0092 was obtained by mating TH27 with JA1403. CAL0135 was constructed in this study. JA1403 and ONA1 were kindly provided by J. Ahringer (University of Cambridge, Cambridge, United Kingdom) and S. Onami (RIKEN, Yokohama, Japan), respectively. The other strains were from the *Caenorhabditis* Genetics Center.

Transgenic Worms. For construction of the CAL0135 strain, the full-length cDNA of *dyrb-1* was amplified by PCR by using the yk1449h04 clone provided by Y. Kohara (National Institute of Genetics, Mishima, Japan). The full-length gene was cloned into the pID3.01B vector, which was provided by G. Seydoux (Johns Hopkins University, Baltimore, MD). Transgenic worms were created using the microparticle bombardment technique (1).

RNAi. RNAi was performed by injecting dsRNAs as described previously (2). dsRNAs were amplified by PCR by using *C. elegans* genomic DNA. Primer sets for amplification of dsRNAs in this study are the same as in PhenoBank (http://www.worm.mpi-cbg.de/phenobank2/cgi-bin/MenuPage.py) except for *tba-1* and *tba-2*. For *tba-1* and *tba-2*, the primer sets described in a previous study (3) was used. Worms injected with dsRNA were incubated at 22 °C for 24 to 30 h before analysis of their embryos. For analysis in *zyg-12*(*ct350*) mutants, worms grown at 16 °C were injected with dsRNA of *dhc-1* or *dyrb-1*, incubated at 16 °C for 24 to 48 h, and shifted to 25 °C for 1 h before analysis.

Microscopy. For staining of lysosomes, L1 worms were transferred to NGM plates containing 4 μM LysoTracker Red (Molecular Probes), and the plates were incubated at 22 °C for 2 d in the dark. For analysis by microscopy, eggs were placed on an agar pad in M9 buffer and covered with a coverslip. Visualization of GFP or mCherry fusion proteins or lysosomes labeled with LysoTracker Red was performed by using a spinning-disk confocal system (CSU10 or CSU-X1; Yokogawa) mounted on a microscope (BX61 or BX71; Olympus) equipped with a UPlanSApo 100× 1.40 NA objective (Olympus) at room temperature. To obtain differential interference contrast images, eggs were viewed with a microscope (BX51; Olympus) equipped with a UPlanSApo 100× 1.40 NA objective at room temperature. Digital images were obtained by using a CCD camera [ORCA-AG (Hamamatsu) or iXon (Andor)] controlled by IPLab software (BD Biosciences).

Quantification of the Movement of Organelles, Pronuclei, and Spindle. For the quantification of the movement of cytoplasmic organelles (early endosomes, lysosomes, and yolk granules), the signals that moved continuously for at least 2 s at a rate of at least 0.5 μm/s in the confocal section containing the centrosomes were used. The candidate signals were first picked up by human eyes and then quantified using MTrackJ of ImageJ software (National Institutes of Health). For measurements of the velocity of the fast phase in female pronuclear migration and centrosome centration velocity, the center positions of the female or the male pronucleus at successive time points were measured by using ImageJ. The average velocity of female pronuclear migration from the onset of acceleration of the migration until pronuclear meeting was determined as the fast-phase velocity of female pronuclear migration. The average velocity of male pronuclear migration from the time the anterior side of the male pronuclear edge reached 20% of EL until the edge reached 50% (the posterior-most side of the egg, 0%) was determined as the centration time. For analysis of spindle rocking movement, the positions of the posterior spindle pole at successive time points were tracked by using ImageJ. The average velocity of the maximum swing was calculated.

Statistical Analysis. A Pearson correlation coefficient test was used to analyze the correlation between organelle movements and centrosome movement (Fig. 5). The statistical difference in Fig. 6 and Fig. S2 was tested with a Student *t* test. The normality of the data were assessed by using the Shapiro–Wilk test. *P* values lower than 0.05 were considered statistically significant.

1. Praitis V, Casey E, Collar D, Austin J (2001) Creation of low-copy integrated transgenic lines in Caenorhabditis elegans. *Genetics* 157:1217–1226.
2. Hara Y, Kimura A (2009) Cell-size-dependent spindle elongation in the Caenorhabditis elegans early embryo. *Curr Biol* 19:1549–1554.
3. Wright AJ, Hunter CP (2003) Mutations in a beta-tubulin disrupt spindle orientation and microtubule dynamics in the early Caenorhabditis elegans embryo. *Mol Biol Cell* 14:4512–4525.

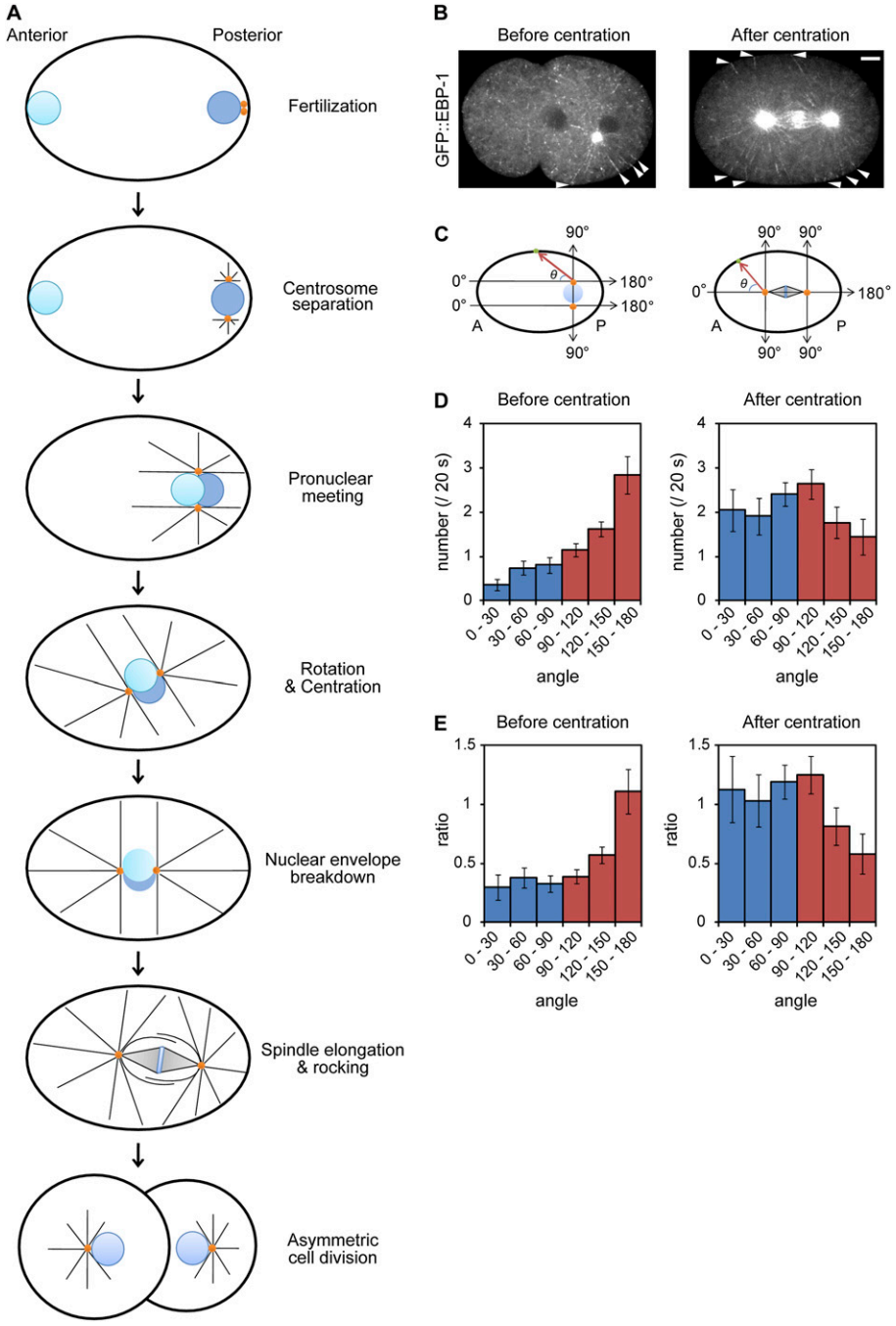

Fig. S1. Schematic representation of the movements of the centrosomes and the number of microtubules reaching the cortex in the one-cell stage *C. elegans* embryo. (*A*) The centrosomes (orange circles) derive from the sperm. The sperm-entry site becomes the posterior side of the embryo. After fertilization, male and female pronuclei form (blue and light blue circles, respectively), and the centrosomes move toward the center of the cell. (*B*) Ten sequential fluorescence images of embryos expressing GFP::EBP-1, which marks the plus-end of microtubules, were projected into a single image to visualize the trajectories of growing microtubules before and after centrosome centration. The images were taken every 1 s. White arrowheads indicate the positions of microtubules that reach the cortex. (Scale bar, 5 μm.) (*C*–*E*) The number of GFP::EBP-1 signals that pass within 1 μm of the cortex was counted for 20 s before and after centrosome centration. (*C*) Counted signals were classified according to angles to the AP axis. (*D*) The average number per centrosome ± SEM is shown ($n \geq 22$). Before centrosome centration, the number of microtubules that reach the cortex in the anterior side of the centrosome (0°–90°) is apparently less than in the posterior side of the centrosome (90°–180°). We counted the number of signals in the confocal sections containing the centrosomes. The chance that the plus-end of a microtubule exits from the confocal section is roughly proportional to the length of the microtubule. To incorporate this effect, the number of microtubules was multiplied by the average length of microtubules in each class and normalized with the mean value of the all classes before and after centration. The normalized number ("ratio") of microtubule reaching the most posterior region (i.e., 150°–180°) was still more than threefold of that reaching each of the anterior region before centration (*E*). It is unlikely that microtubule pulling at the anterior cortex is stronger than that at the posterior cortex. This observation challenges the idea that the cortical pulling forces drive centrosome centration.

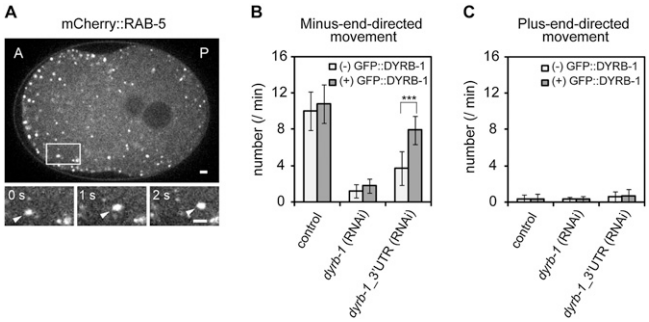

Fig. S2. Movements of RAB-5–containing vesicles. (*A*) Tracking of RAB-5 puncta, some of which move directionally as shown in the lower magnified images. (Scale bars, 2 μm.) (*B* and *C*) The frequency of fast (≥0.5 μm/s) and continuous (≥2 s) movements of RAB-5 puncta toward the minus end (*B*) or plus end (*C*) of the microtubules was counted for 2 min after pronuclear meeting. The average number ± SD per 1 min is shown. A statistically significant difference is indicated by the asterisks (***$P < 0.001$). The minus end-directed movements of RAB-5 vesicles were inhibited by RNAi of *dyrb-1*. *gfp::dyrb-1* construct, which do not contain 3′-UTR sequence of native *dyrb-1* gene, partially rescued the defect caused by RNAi targeting 3′-UTR of *dyrb-1*, indicating GFP::DYRB-1 fusion protein used in this study is functional.

Table S1. Results of screening for genes involved in centration by use of the PhenoBank database

	Gene	Name	No. of videos*	Score, %†
1	F55H2.3/2.4	*lrg-1*	12/12	100
2	ZK593.5	*dnc-1*	7/11	64
3	F08B6.2	*gpc-2*	6/10	60
4	F13D12.7	*gpb-1*	6/10	60
5	C28H8.12	*dnc-2*	7/12	58
6	C29E4.8	*let-754*	6/11	55
7	Y53F4B.22	*arp-1*	5/10	50
8	T24H10.6	*dyrb-1*	5/10	50
9	Y59A8A.1	*csn-1*	5/10	50
10	T26A5.8	—	18/37	49
11	C36E8.5	*tbb-2*	10/22	45
12	K08E7.3	*let-99*	4/9	44
13	T03F6.5	*lis-1*	3/7	43
14	Y49E10.15	*snr-6*	5/12	42
15	C26B2.1	*(p62)*	4/10	40
16	F26E4.8	*tba-1*	4/10	40
17	Y108G3AL.1	*cul-3*	4/10	40
18	F49E11.1	*mbk-2*	6/15	40
19	Y71F9AL.14	*(p25)*	5/13	38
20	F01F1.12	—	6/17	35
21	T16G12.1	—	4/12	33
22	Y39G10AR.12	*tpxl-1*	3/9	33
23	T06G6.9	*pfd-3*	5/15	33
24	F26E4.1	*sur-6*	3/9	33
25	D2024.6	*cap-1*	3/10	30
26	C47B2.3	*tba-2*	3/10	30
27	ZK858.4	*mel-26*	4/15	27
28	C39E9.14	*dli-1*	2/8	25
29	C54C6.2	*ben-1*	2/9	22
30	F10G7.8	*rpn-5*	2/9	22
31	K01G5.7	*tbb-1*	3/14	21
32	F44F4.11	*tba-4*	5/24	21
33	F22B5.7	*zyg-9*	1/5	20
34	F36A4.7	*ama-1*	3/15	20
35	F14B8.1	*nhx-4*	3/15	20
36	ZK637.8	*unc-32*	2/13	15
37	C25A1.9	*rsa-1*	2/14	14
38	K01C8.10	*cct-4*	1/9	11
39	C14B9.4	*plk-1*	7/63	11
40	C17H12.1	*dyci-1*	1/10	10
41	T21E12.4	*dhc-1*	1/10	10
42	F54B3.3	—	1/10	10
43	Y71H2B.3	*ppfr-3*	2/23	9
44	ZK287.5	*rbx-1*	1/12	8
45	C39B5.2	—	1/12	8
46	T26A5.9	*dlc-1*	1/14	7
47	C08B11.1	*zyg-11*	1/14	7
48	Y19D2B.1	—	0/5	0
49	Y54E2A.3	*tac-1*	0/5	0
50	F56A3.4	*spd-5*	0/11	0
51	F57B1.2	*sun-1*	0/11	0
52	F56A3.3	*npp-6*	0/9	0
53	C08F8.1	*pfd-1*	0/15	0
54	W02D3.9	*unc-37*	0/19	0
55	F58A6.5	—	0/7	0
56	E04A4.4	*hoe-1*	0/3	0

All videos (N = 726) of the 56 genes categorized into the "P0 Pronuclear centration" or "P0 Pronuclear Migration (male)" defect groups in PhenoBank were checked for centration and pronuclear meeting. The number of videos displaying the centration defect but not the pronuclear meeting defect was counted.
*The number of videos displaying the centration defect but not the pronuclear meeting defect/the total number of videos in each gene. Still shots were not included in our results.
†The percentage of videos displaying the centration defect but not the pronuclear meeting defect/the total number of videos in each gene.

Table S2. Centrosome centration defect in *dyrb-1* (RNAi) embryos is not due to a defect in centrosome separation

Genotype	CS defect*	Score, %[†]
Control	0/8	0
dnc-2 (RNAi)	3/8	38
arp-1 (RNAi)	4/9	44
dyrb-1 (RNAi)	0/9	0
dnc-2 (RNAi);*gpr-1/2* (RNAi)	11/12	92
arp-1 (RNAi);*gpr-1/2* (RNAi)	8/10	80
dyrb-1 (RNAi);*gpr-1/2* (RNAi)[‡]	1/13	8
rab-5 (RNAi)	0/6	0
rab-7 (RNAi)	0/7	0
rilp-1 (RNAi)	0/6	0

CS, centrosome separation.

*The number of embryos displaying the CS defect/the total number of embryos in each genotype.

[†]CS defect ratio in percentage terms.

[‡]A previous report showed that RNAi of *dyrb-1* in a *gpr-1*(or574ts) background, which is a weak loss-of-function allele of *gpr-1*, causes a centrosome separation defect at a frequency of 60% (1). In our experiment of simultaneous disruption of DYRB-1 and GPR-1/2 by RNAi, we did not observe a significant centrosome separation defect.

1. Couwenbergs C, et al. (2007) Heterotrimeric G protein signaling functions with dynein to promote spindle positioning in C. elegans. *J Cell Biol* 179:15–22.

Table S3. Number of GFP::DYRB-1 puncta

Genotype	Total no.*	Minus end[†]	Plus end[†]	No.
Control	32.4 ± 6.3	2.3 ± 0.6	0.7 ± 0.2	10
tba-1/2 (RNAi)	46.7 ± 17.5	0.6 ± 0.3	0.2 ± 0.2	10

*Total number of GFP::DYRB-1 puncta in equatorial confocal sections. The average number ± SD is shown.

[†]Number of GFP::DYRB-1 puncta that moved continuously for at least 2 s at a rate ≥ 0.5 μm/s toward the minus end or plus end of the microtubules in the sections. The average number ± SEM per 30 s is shown. We regarded the position of the centrosome or the male pronucleus as the minus-end direction of the microtubules.

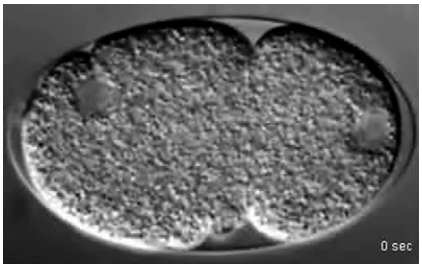

Movie S1. Pronuclear migration and spindle rocking in the WT. Time-lapse Nomarski differential interference contrast microscopy image of fertilized *C. elegans* embryo is shown. The pronuclei and mitotic spindle can be detected as smooth objects within the cell. The pronuclei moves to the cell center, and the mitotic spindle shows oscillatory rocking behavior as described in Fig. S1*A*.

Movie S1

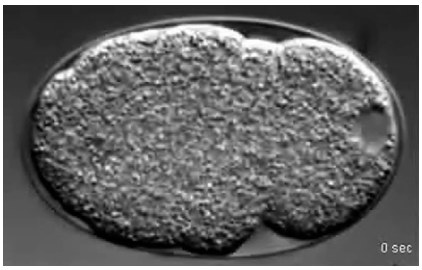

Movie S2. Pronuclear migration and spindle rocking in *gpr-1/2* (RNAi) embryo. Same as Movie S1 but *gpr-1/2* were knocked down. GPR-1/2 functions with the cortical fraction of DYRB-1 to produce microtubule-pulling forces from the cortex. The rocking of the spindle is significantly inhibited in the embryo, whereas the centration of the pronucleus is normal (or speeds up).

Movie S2

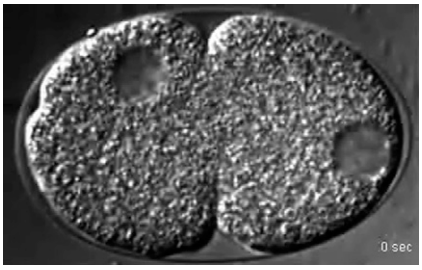

Movie S3. Pronuclear migration and spindle rocking in *dyrb-1* (RNAi) embryo. Same as Movie S1 but *dyrb-1* function was knocked down by RNAi. The two pronuclei meet but they do not complete centration. The rocking of the spindle is also defective.

Movie S3